An atypical catalytic mechanism involving three cysteines of thioredoxin

Cha San Koh, Nicolas Navrot, Claude Didierjean, Nicolas Rouhier, Masakazu Hirasawa, David B. Knaff, Gunnar Wingsle, Razip Samian, Jean-Pierre Jacquot, Catherine Corbier, et al.

THE JOURNAL OF BIOLOGICAL CHEMISTRY VOL. 283, NO. 34, pp. 23062–23072, August 22, 2008

An Atypical Catalytic Mechanism Involving Three Cysteines of Thioredoxin*[S]

Received for publication, March 17, 2008, and in revised form, June 13, 2008 Published, JBC Papers in Press, June 14, 2008, DOI 10.1074/jbc.M802093200

Cha San Koh[‡§1], Nicolas Navrot[¶‖], Claude Didierjean[‡], Nicolas Rouhier[¶], Masakazu Hirasawa[**], David B. Knaff[**], Gunnar Wingsle[‖], Razip Samian[§], Jean-Pierre Jacquot[¶], Catherine Corbier[‡‡], and Eric Gelhaye[¶2]

*From the [‡]LCM3B, Equipe Biocristallographie, UMR 7036 CNRS-Université Henri Poincaré, [¶]Unité Mixte de recherche INRA-UHP 1136, Interactions Arbres/Micro-organismes, [‡‡]URAFPA, Equipe PB2P, Faculté des Sciences et Techniques, Nancy Université, BP 239, 54506 Vandoeuvre Cedex France, the **Department of Chemistry and Biochemistry, and Center for Biotechnology and Genomics, Texas Tech University, Lubbock, Texas 79409-1061, the [§]School of Biology, Universiti Sains Malaysia, Minden, 11800 USM, Penang, Malaysia, and the [‖]Department of Forest Genetics and Plant Physiology, Faculty of Forestry, Swedish University of Agricultural Sciences, SE-901 83 Umea, Sweden*

Unlike other thioredoxins *h* characterized so far, a poplar thioredoxin of the *h* type, PtTrx*h*4, is reduced by glutathione and glutaredoxin (Grx) but not NADPH:thioredoxin reductase (NTR). PtTrx*h*4 contains three cysteines: one localized in an N-terminal extension (Cys^4) and two (Cys^{58} and Cys^{61}) in the classical thioredoxin active site ($^{57}WCGPC^{61}$). The property of a mutant in which Cys^{58} was replaced by serine demonstrates that it is responsible for the initial nucleophilic attack during the catalytic cycle. The observation that the C4S mutant is inactive in the presence of Grx but fully active when dithiothreitol is used as a reductant indicates that Cys^4 is required for the regeneration of PtTrx*h*4 by Grx. Biochemical and x-ray crystallographic studies indicate that two intramolecular disulfide bonds involving Cys^{58} can be formed, linking it to either Cys^{61} or Cys^4. We propose thus a four-step disulfide cascade mechanism involving the transient glutathionylation of Cys^4 to convert this atypical thioredoxin *h* back to its active reduced form.

Thioredoxins (Trxs)[3] are small molecular weight proteins found in all organisms from prokaryotes to higher eukaryotes. They are involved in many cellular processes, dealing primarily with cell redox regulation. In plants, numerous isoforms have been reported. For example, at least 20 genes coding for Trxs are present in the completely sequenced genome of *Arabidopsis thaliana* (1). The Trxs *f*, *m*, *x*, and *y* are present in chloroplasts (2, 3), whereas the Trxs *o* are localized in mitochondria (4). The Trxs *h* constitute a large group that includes cytosolic and mitochondrial isoforms (1, 5–7). Trxs *h* have been divided in three distinct subgroups in a classification based on their primary structure (5). Members of the first and second groups are reduced by NADPH in a reaction catalyzed by NTR. Members of the first and second Trxs *h* subgroups contain a conserved WC(G/P)PC catalytic site. The first cysteine is the one involved in the nucleophilic attack on disulfide bonds present in target proteins, leading to the formation of a disulfide bond between the target protein and Trx. This intermolecular disulfide is then reduced by the second cysteine, leading to the release of reduced target protein and oxidized Trx.

It is only recently that members of plant Trx *h* subgroup 3 have been detected and characterized, with much of the evidence coming from studies on poplar (8, 9). The poplar thioredoxin PtTrx*h*4, which belongs to this subgroup, contains a typical WCGPC catalytic site but differs from previously characterized Trxs *h* in being reduced *in vitro* by glutaredoxins but not by NTR (8). This unique feature raised several questions about the reaction mechanism of PtTrx*h*4. For example, as most characterized Trxs have a redox midpoint potential of about −290 mV, whereas Grxs are more electropositive (about −200 mV), questions about the thermodynamic favorability of reduction of a Trx-like molecule by Grx naturally arise.

The structural and redox properties of animal, bacterial, and some plant Trxs have been studied extensively, but little structural information about higher plant Trx *h* is available (10, 11). In addition, there is no subgroup 3 Trx *h* structure solved to date. Because members of this subgroup exhibit an N-terminal extension containing a conserved cysteine in the fourth position that is absent in other subgroups, questions concerning the role of this extension and its additional cysteine arise. It is of particular interest to know how this extension is positioned with respect to the conserved Trx fold and more importantly to understand why this protein does not react with its traditional reducing partner, NTR. We show here that, in contrast to other Trxs, three cysteines rather than two are involved in the catalytic mechanism of PtTrx*h*4. Two of these cysteines are present in the classical Trx catalytic site ($WC^{58}GPC^{61}$), whereas the third one is localized in the N-terminal extension (Cys^4). From

* This work was supported in part by Grant D-0710 (to D. B. K.) from the Robert A. Welch Foundation. The costs of publication of this article were defrayed in part by the payment of page charges. This article must therefore be hereby marked "*advertisement*" in accordance with 18 U.S.C. Section 1734 solely to indicate this fact.

The atomic coordinates and structure factors (code 3D21 and 3D22) have been deposited in the Protein Data Bank, Research Collaboratory for Structural Bioinformatics, Rutgers University, New Brunswick, NJ (http://www.rcsb.org/).

[S] The on-line version of this article (available at http://www.jbc.org) contains supplemental Fig. S1.

[1] Recipient of the ASTS (Academic Staff Training Scheme) fellowship from the Universiti Sains Malaysia.

[2] To whom correspondence should be addressed: Unité Mixte de recherche INRA-UHP 1136, Interactions Arbres/Micro-organismes, Faculté des Sciences et Techniques, Nancy Université, BP 239, 54506 Vandoeuvre Cedex France. Tel.: 33-0-3-83-68-42-28; E-mail: gelhaye@lcb.uhp-nancy.fr.

[3] The abbreviations used are: Trx, thioredoxin; Grx, glutaredoxin; NTR, NADPH thioredoxin reductase; Prx, peroxiredoxin; DTT, dithiothreitol; SeMet, selenomethionine; WT, wild type.

the kinetic and structural data, a new catalytic mechanism is proposed for this Trx isoform.

EXPERIMENTAL PROCEDURES

Cloning and Mutations of PtTrxh4—The procedures for cDNA isolation of PtTrx*h*4 and its subsequent cloning are described in Ref. 8. The PtTrx*h*4 mutants C4S, C58S, and C61S were generated by PCR using cloning and mutagenic oligonucleotides shown below (NcoI and BamHI sites are underlined and mutagenic bases are in bold): PtTrx*h*4 direct, 5′-CCCCCCATGGGACTTTGCTTGGAT-3′; and PtTrx*h*4 reverse, 5′-CCCCGGATCCTCATTTGTCACTAGGGGGCAA-3′; PtTrx*h*4C4S direct, 5′-CCCCCCATGGGACTT**AGC**TTGGATAAGCAT-3′; PtTrx*h*4C58S direct, 5′-TTCAGTGCAACATGGAGTGG-**TCC**TTGTAGACAG-3′; PtTrx*h*4C58S reverse, 5′-CTGTCTACAA**GGA**CCACTCCATGTTGCACTGAA-3′; PtTrx*h*4C61S direct, 5′-ACATGGTGTGGTCCT**AGT**AGACAGATTGCACCG-3′; and PtTrx*h*4C61S reverse, 5′-CGGTGCAATCTGTCT**ACT**AGGACCACACCATGT-3′.

The mutated PCR products that contained the restriction sites have been cloned into expression plasmid pET-3d, yielding constructions pET PtTrx*h*4C4S, pET PtTrx*h*4C58S, and pET PtTrx*h*4C61S. The mutations of the recombinant plasmids were verified by DNA sequencing.

Expression and Purification of the Recombinant Proteins—All procedures for the expression and purification of *Arabidopsis thaliana* NTR B (AtNTRB), poplar PrxQ (PtPrxQ), and Grx (WT and mutants) are described elsewhere (12–15). All the PtTrx*h*4 proteins have been expressed in *Escherichia coli* strain BL21(DE3), which was also co-transformed with the plasmid helper pSBET as described in Ref. 16. The [SeMet]PtTrx*h*4 gene was amplified from a *P. tremula* × *tremuloides* cDNA library. The gene was inserted in the pET-3d expression plasmid, between NcoI and BamHI sites. Recombinant plasmids carrying the gene of interest were electroporated into the methionine auxotrophic strain of *E. coli* BL21(DE3) pSBET. Bacteria were cultured in M9 medium supplemented with selenomethionine (SeMet) and protein overexpression performed as previously described (17). Mass spectrometry was performed to assess purity and to confirm the full incorporation of SeMet, all purification steps of the mutated PtTrx*h*4 proteins being similar to those described for PtTrx*h*4 in Ref. 8.

Thiol Content Titration—The thiol content of each protein preparation was measured using the dithionitrobenzoate (DTNB) procedure as described in Ref. 14. All thiol titrations were performed in the presence of SDS on enzymes either as purified or after dithiothreitol (DTT) reduction and dialysis. Consequently, all thiols are titrated regardless of whether or not they were accessible in the protein.

Glutathionylation Experiments—The reaction mixture (50 μl) containing 30 mM Tris-HCl, pH 8.0, 1 mM 1,4-DTT, and 50 μg of poplar Trx (concentration about 80 μM) was incubated for 10 min before adding 5 mM oxidized glutathione.

Electrospray Mass Spectrometry—A Micromass Q-TOF Ultima (Waters Micromass MS Technologies) hybrid tandem mass spectrometer was used for the acquisition of the electrospray ionization (ESI) mass spectra. This instrument is equipped with a nanoflow electrospray source. The samples were infused into the mass spectrometer using nanoflow capillaries (Proxeon Biosystems, Denmark). The needle voltage was ~1800 V, and the collision energy was 10 eV for the MS analyses. Samples for flow injection analyses were diluted 1:20 with a solution of 50:50 acetonitrile, 0.1% formic acid. Data analysis was accomplished with a MassLynx data system and Transform deconvolution software supplied by the manufacturer (Waters Micromass MS Technologies).

Redox Potential Determination—Oxidation-reduction titrations were carried out as described previously using the fluorescence of the monobromobimane-modified form of the reduced protein to monitor the extent of the reduction of the protein (18, 19). Ambient potentials (E_h) were established using mixtures of oxidized glutathione (GSSG) and reduced glutathione (GSH) and the PtTRX*h*4 samples were incubated at these defined E_h values for 2 h to reach redox equilibrium. The oxidation-reduction midpoint potential (E_m) value was shown to be independent of the total concentration (GSSG and GSH) present in the redox equilibration buffer over the range from 2 to 5 mM. The E_m was calculated by fitting the data to the Nernst equation for a two-electron process as described previously (20).

PrxQ Activity Measurement—The reduction of H_2O_2 by poplar PrxQ in the presence of PtTrx*h*4 was followed spectrophotometrically, using a Cary 50 spectrophotometer, by monitoring the decrease in absorbance arising from NADPH oxidation in a coupled enzyme assay system. The reaction mixture (500 μl) contained 30 mM Tris-HCl, pH 8.0, 1 mM EDTA, 200 μM NADPH, 0.5 IU glutathione reductase, 1 mM GSH, 6 μM PtGrx C4, 16 μM PtTrx*h*4 WT and mutants, 500 μM H_2O_2, and 2 μM PtPrxQ.

Alternatively, H_2O_2 disappearance was followed directly. The reaction mixture (100 μl) contained 30 mM Tris-HCl, pH 7.0, 500 μM DTT, 4 μM PtPrxQ, and 36 μM PtTrx*h*4. The reaction was started by adding 500 μM H_2O_2. After given incubation times, 5 μl were mixed with 495 μl of FOX1 (ferrous oxidation in xylenol orange) reagent (21). The absorbance was then read at 560 nm after 1-h incubation.

Crystallization—Three different samples were crystallized, one with Se-Met (WT PtTrx*h*4) and two with regular methionines (WT and PtTrx*h*4C61). Crystallization conditions were screened extensively at 20 °C with the microbatch method. Drops used for the initial crystallization trials consisted of 2 μl of the protein solution (20 mg/ml) mixed with 2 μl of various crystallization solutions. The [SeMet]PtTrx*h*4 crystals were grown in 1.0 M sodium/potassium phosphate buffer, pH 6.9, (Hampton SaltRx Screen 2, solution 54), whereas the WT PtTrx*h*4 was obtained by using the JBS screen 2 solution D2 (30% PEG 4000, 0.1 M NaHEPES, pH 7.5, 0.2 M $CaCl_2$).

For PtTrx*h*4C61S protein, orthorhombic crystals were obtained by using the Hampton SaltRx Screen condition 55 buffer (1.0 M sodium/potassium phosphate, pH 8.2). The drop was formed by mixing 25 mg/ml protein with crystallization solution in a 1:1 ratio. Crystals were cryoprotected and flash-cooled in liquid ethane at 100 K.

Data Collection and Processing, Structure Solutions, and Refinements—Information and statistics of data collection and processing of the three crystals are presented in Table 1. The

TABLE 1
Data collection, phasing, and refinement statistics for the [SeMet]PtTrx*h*4, the WT PtTrx*h*4, and the PtTrx*h*4C61S crystals

Data set	[SeMet]PtTrx*h*4	WT PtTrx*h*4	PtTrx*h*4 C61S
Data collection and processing statistics			
Data collection site	BM30A ESRF-Grenoble	X11 DESY-Hamburg	BW7A DESY-Hamburg
Wavelength (Å)	0.9805	0.8123	1.2400
Space group	$P4_12_12$	$P6_1$	$P2_12_12_1$
Unit cell dimensions (Å) (*a*, *b*, *c*)	44.89, 44.89, 131.74	47.35, 47.35, 196.00	31.78, 44.10, 85.68
Asymmetric unit	1 subunit	2 subunits	1 subunit
Resolution range (Å)[a]	32.94–2.46 (2.60–2.46)	50.00–2.15 (2.23–2.15)	30.00–1.60 (1.66–1.60)
Redundancy[a]	7.0 (3.6)	28.3 (37.6)	5.2 (5.3)
Completeness (%)[a]	93.4 (65.7)	99.8 (100.0)	98.5 (98.4)
$I/\sigma I$[a]	17.85 (3.10)	22.98 (2.60)	16.03 (6.20)
R_{merge}[a,b]	0.089 (0.588)	0.053 (0.392)	0.092 (0.266)
Phasing power (acentric/centric)	1.283/0		
R_{cullis} (isomorphous/anomalous)	0/0.754		
Figure of merit (acentric/centric)	0.34824/0.06270		
Refinement statistics			
Resolution range (Å)		41.0–2.15	30.0–1.6
Reflections used		12,725	15,470
R_{cryst}[c] (R_{free})[d]		20.97 (28.53)	19.06 (19.63)
Protein/waters/PO_4		2 × (111 residues)/63/0	129 residues/115/1
Mean *B* factor (Å^2)			
Main chain		55.20	19.40
Side chain		57.67	21.52
Water		59.29	32.47
All		56.53	21.69
Rms deviation from ideal geometry			
Bond lengths (Å)		0.030	0.010
Bond angles (°)		2.5	1.4
Dihedral angles (°)		26.3	24.1
Improper angles (°)		5.59	1.46
Ramachandran plot			
Residues in most favored regions (%)		91.5	92.8
Residues in additionally allowed regions (%)		7.5	7.2
Residues in generously allowed regions (%)		1.0	0.0

[a] The values in parentheses are for the highest resolution bin.
[b] $R_{merge} = \Sigma_i|I_i - \text{bIN}|/\Sigma|\text{bIN}|$, where *I* is the intensity for the ith measurement of an equivalent reflection with the indices *h*, *k*, *l*.
[c] $R_{cryst} = \Sigma||F_o| - |F_c||/\Sigma|F_o|$, where F_o and F_c are the observed and calculated structure factor amplitudes, respectively.
[d] The R_{free} value was calculated from 5% of all data that were not used in the refinement.

diffraction images of the different crystals were indexed, integrated, and scaled using either the HKL program (22) or the XDS program package (23), then analyzed using the CCP4 software package version 6.0.2 (24).

A SeMet-labeled protein was prepared and a single-wavelength anomalous dispersion dataset was collected. Although three selenium atoms per protein were expected (including the one associated to the first methionine residue), only two were found ($SeMet^{79}$ and $SeMet^{134}$) using *SHELXL*97 (25). Subsequent mass spectroscopy analysis allowed us to identify a SeMet-labeled protein that is presumed to be truncated (113 instead of 139 amino acids; absence of the N-terminal part) during its production in the *E. coli* system. The solution with the highest correlation coefficient in the heavy atom position determination was fed into SHARP (26) for further refinement of SeMet-sulfur positions and phasing. After refinement, SHARP reported that occupancies of heavy atoms were 1.0, respectively, and the calculated experimental phase had an overall figure of merit of 0.35 (acentric reflections) and 0.06 (centric reflections) for 35-2.5-Å diffraction data. The phase improvement was made using SOLOMON (27) where the figure of merit gradually increased to 0.79 and the electron density map became interpretable. This map was submitted to the automatic model building program ARP/wARP, version 6.1 (28), and 95 residues of the expected 113 were built. The initial model was further improved by manual building with Turbo-Frodo (29) or Coot (30) interspersed with refinements using both CNS, version 1.1 (31), and REFMAC5 (24).

Models of the wild type and the PtTrx*h*4C61S mutant were solved by molecular replacement (MOLREP) (32) using [SeMet]PtTrx*h*4 as the search model. The final structure of the WT PtTrx*h*4 was obtained after manual rebuilding of many parts of the structure (mainly near the active site and the α-helix 3 regions) and refinements using CNS and REFMAC5. Concerning the PtTrx*h*4C61S mutant, 82% of the model was built automatically using ARP/wARP. The final mutant model was obtained using the same procedure used for the WT protein. Throughout the model building and refinement processes, qualities of all models were assessed using the program PROCHECK (33). Refinement statistics are summarized in Table 1. Figures were prepared with PyMOL (34).

Structure Superimpositions—Superimpositions of the present structures with their homologous structures obtained from the Protein Data Bank were performed using the LSQMAN program from the DEJAVU package (35), and the Lsqkab (superpose) program of the CCP4 suite with default parameters proposed by the authors.

Protein Data Bank Accession Codes—Atomic coordinates and structure factors have been deposited in the Protein Data Bank. Accession codes are 3D21 (WT PtTrx*h*4) and 3D22 (PtTrx*h*4C61S).

RESULTS

PtTrx*h*4 belongs to the third Trx *h* subgroup and exhibits the classical WCGPC active site. In addition to these two cysteinyl residues, members of this subgroup contain one additional con-

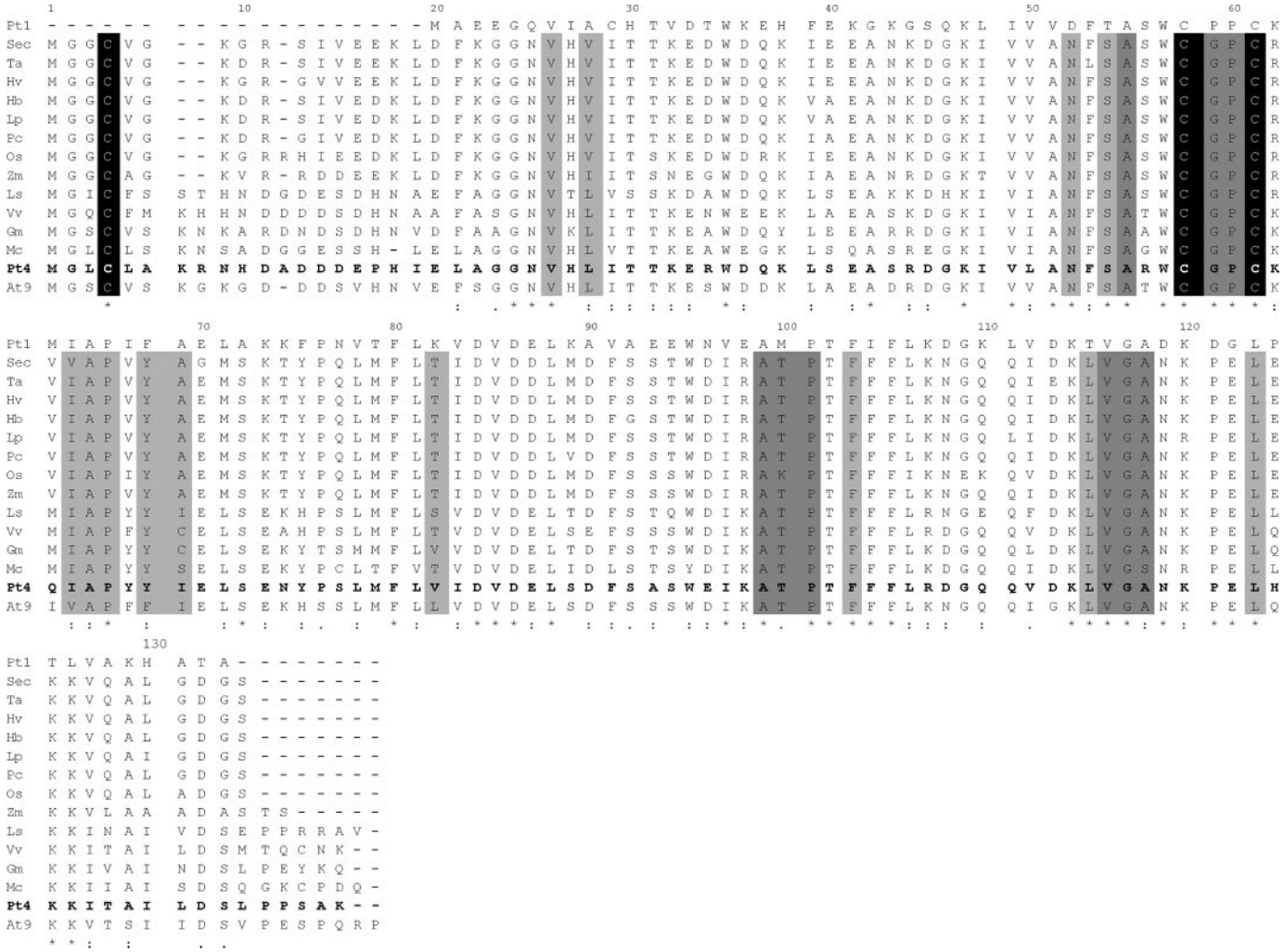

FIGURE 1. **Multiple alignment of poplar Trx*h*4-related sequences.** Amino acid sequences were aligned using CLUSTALW software. Accession numbers are as follows: *Pt1*, *Populus tremula* × *Populus tremuloides* (AAL99941); *Sec*, *Secale cereale* (AF159386); *Ta*, *Triticum aestivum* (AF438359); *Hv*, *H. vulgare* (AF435815); *Hb*, *Hordeum bulbosum* (AF159385); *Lp*, *Lolium perenne* (159387); *Pc*, *P. coerulescens* (AF159388); *Os*, *Oryza sativa* (AF435817); *Zm*, *Zea mays* (AF435816); *Ls*, *Lactuca sativa* (TC9851); *Vv*, *Vitis vinifera* (CB004453); *Gm*, *Glycine max* (CA799351); *Mc*, *Mesembryanthemum crystallinum* (CA838461); *Pt4*, *P. tremula* × *P. trichocarpa* (P85801); *At9*, *A. thaliana* (At3g08710). The *asterisk* corresponds to strict identity, the *colon* corresponds to functional homology, and the *period* corresponds to structural homology. Amino acids that compose hydrophobic sites 1 and 2 are highlighted in *dark gray* and *light gray*, respectively. Three cysteines proposed to be involved in the atypical catalytic mechanism of PtTrx*h*4 (see text for details) are well conserved in its orthologs (shown in "*black*").

served cysteine found in the fourth position in an N-terminal extension (comprising the 24 most N terminus residues) (Fig. 1). Sequence analysis using several localization prediction programs suggests that the N-terminal extension does not correspond to a signal peptide and that this protein is likely to be located in the cytosol.

Thiol Content Determination—To investigate the putative role of the three conserved cysteines in the catalytic mechanism of PtTrx*h*4, site-directed mutagenesis has been used to produce the full-length recombinant proteins in *E. coli*: PtTrx*h*4C4S, PtTrx*h*4C58S, and PtTrx*h*4C61S. Thiol content of these proteins has been determined both in reducing and non-reducing conditions. A summary of these data is shown in Table 2. Nearly three thiols per protein are titrated for the reduced WT protein, whereas approximately one SH group is present in the unreduced WT protein. Under reducing conditions, thiol contents of the PtTrx*h*4C4S, PtTrx*h*4C58S, and PtTrx*h*4C61S mutants were all close to 2 SH/mol in good agreement with the expected theoretical values. In the absence of reductant, the

TABLE 2

Thiol content of PtTrx*h*4 under nonreducing or reducing conditions

Thiols were titrated using DTNB as described under "Experimental Procedures." Data are expressed in mole of SH/mole of enzyme. The S.D. is typically ± 0.2 SH/mol of SH.

	Nonreducing conditions	Reducing conditions
WT PtTrx*h*4	0.75	2.88
PtTrx*h*4C4S	0.93	1.64
PtTrx*h*4C58S	0.64	1.93
PtTrx*h*4C61S	0.05	1.55

PtTrx*h*4C61S mutant is fully oxidized (no titrated thiol group), whereas PtTrx*h*4C4S and PtTrx*h*4C58S mutants are only partially oxidized (*i.e.* thiol content values lower than 1 SH/mol were measured).

SDS-PAGE was performed under reducing and non-reducing conditions (see supplementary data Fig. S1). In the absence of DTT, both monomers and dimers were detected for PtTrx*h*4 WT and C61S with monomers being the dominant species for both proteins. Although thiol titration results are most consist-

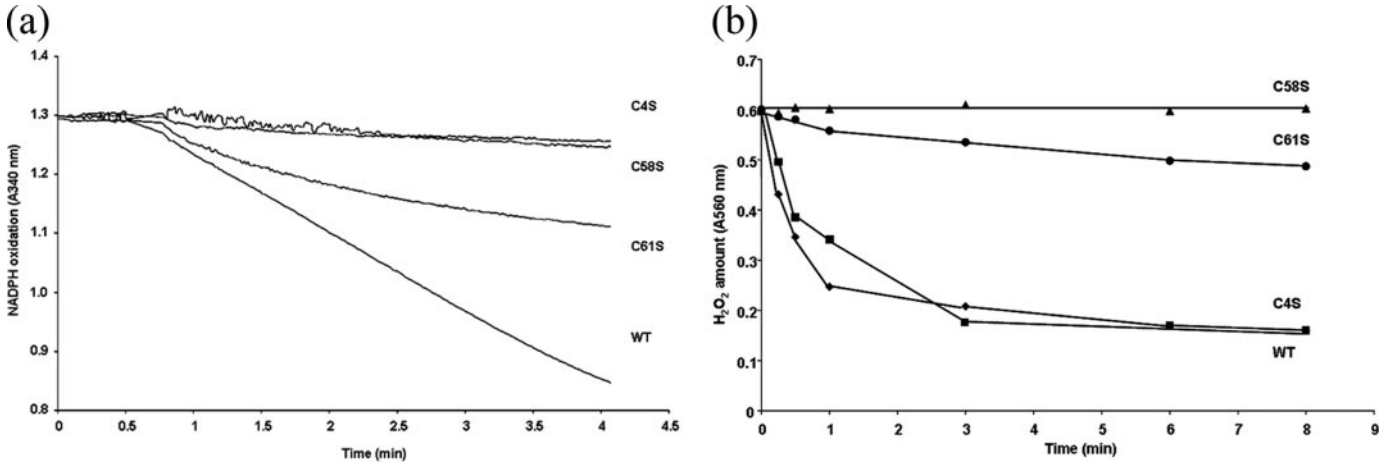

FIGURE 2. **Activity of PtTrx*h*4 with PtGrx C4 (*a*) or with DTT (*b*).** For assay in *a*, PtPrxQ (2 μM) was incubated with either PtTrx*h*4WT or the different mutants (16 μM) in the presence of the GSH/Grx system (200 μM NADPH, 1 mM GSH, 0.5 IU glutathione reductase, 6 μM PtGrx C4, 500 μM H_2O_2). NADPH oxidation was measured at 340 nm as absorbance change per min. For assay in *b*, the reduction of H_2O_2 by PtPrxQ (5 μM) was measured by following the disappearance of 500 μM H_2O_2 using 1 mM DTT in the presence of either PtTrxh4WT or the different mutants (30 μM). Depletion of H_2O_2 was measured at 560 nm as absorbance change per min.

ent with the formation of an intramolecular disulfide bond, the presence of reducible dimers for the C61S mutant indicates that Cys^{58} and/or Cys^{4} could be also involved in intermolecular disulfide bonds. Only monomers were observed for the C4S mutant in the absence of DTT, suggesting that an intramolecular disulfide bond is formed between Cys^{58} and Cys^{61}. In the case of the C58S mutant, oligomeric forms (disappearing under reducing conditions) were present in high abundance, which is consistent with the presence of intermolecular disulfide bonds involving Cys^{4} and/or Cys^{61}.

Redox Potential Determination—The redox titrations of PtTrx*h*4 and of its three C/S variants have been carried out at pH 7.0 over the potential range of −50 to −250 mV. Each result represents the average of at least two determinations and the average deviations suggest that the experimental uncertainty in E_m is between 5 and 10 mV. The data obtained for the PtTrx*h*4 and PtTrx*h*4C61S give a good fit to the curve expected for a single two-electron process with an E_m value of −165 ± 10 and −178 ± 10 mV, respectively. Data from redox titrations of PtTrx*h*4C4S and PtTrx*h*4C58S could not be fitted to the Nernst equation for a single two-electron process but did give good fits for the sum of the Nernst equation for two separate two-electron processes. In the case of PtTrx*h*4C4S, the E_m values for the two components are −140 ± 10 and −200 ± 10 mV and for PtTrx*h*4C58S the E_m values of the two components are −130 ± 10 and −180 ± 10 mV. The two-electron nature of these redox couples, the E_h range over which they titrate and the fact that the experiments rely on a thiol-specific reagent, monobromobimane, to monitor the course of the titrations leave little doubt that the components being titrated are dithiol/disulfide couples.

As the redox titration were carried out using the GSH/GSSG couple for redox buffering, it may be possible that some of the components of the redox titration arise from protein-GSH adducts. To investigate the susceptibility of PtTrx*h*4 to glutathionylation, the protein was reduced by DTT, incubated with a large excess of GSSG, and analyzed by quadrupole time-of-flight mass spectrometry. It showed the formation of a low-amplitude peak with a mass of 15,761.00 Da (around 35% of the total preparation) in addition to the peak corresponding to the oxidized recombinant PtTrx*h*4 (15,455.125 Da). This additional peak is compatible with the addition of one GSH molecule (305.5 Da). Concerning the mutants, a large amplitude additional peak (around 90% of the total preparation) corresponding to a GSH adduct was detected with PtTrx*h*4C58S; PtTrx*h*4C61S was glutathionylated to a lesser extent (around 35% of the total preparation); whereas PtTrx*h*4C4S showed no detectable glutathionylation. To identify the glutathionylation site(s) of the WT protein, we performed tryptic digestion of fully reduced or GSSG-oxidized protein and analyzed the tryptic fragments by mass spectrometry. The data indicated that Cys^{4} is the glutathionylation site on PtTrx*h*4, a result consistent to the absence of GSH adduct formation with PtTrx*h*4C4S.

Due to the possibilities of extensive glutathionylation and the multiplicity of possible disulfides (both intra- and intermolecular), the potential redox values obtained are actually the average values of a mixture of disulfides. Hence, it is not yet possible to provide a unique assignment of each E_m component in these two-component titrations. Nevertheless, we can conclude that the redox midpoint potential values for all of the couples involved are more positive than −200 mV, a value that is very much more electropositive than the redox potential of typical Trxs (about −300 mV).

PrxQ Activity—The activity of the recombinant proteins was tested using a non-physiological PrxQ-based system involving PtPrxQ, GSH, and PtGrx (type C4 with an active site CPYC) (8). Both PtTrx*h*4C4S and PtTrx*h*4C58S are totally inactive in this system, whereas the mutant PtTrx*h*4C61S retained some of the activity exhibited by WT PtTrx*h*4 (Fig. 2*a*). Taking into account the data reported from previously characterized Trxs, Cys^{58} is most likely the catalytic residue. As sequence comparisons suggest that Cys^{58} and Cys^{61} are the active site residues (with Cys^{58} making the initial nucleophilic attack characteristic of Trxs), it is not surprising that converting either of these cysteine residues to serine results in loss of activity. The most interesting feature of PtTrx*h*4, based on the observed total loss of activity

for the PtTrx*h*4C4S mutant, is that three cysteines seem to be involved in the catalytic mechanism.

The interactions between PtTrx*h*4 and several PtGrx mutants have also been investigated using this assay. The PtGrx C27S mutant, in which the catalytic cysteine of PtGrx C4 has been replaced to serine, is not active. In this system, mutations of residues surrounding the Grx catalytic cysteines (Y26A and Y29F) altered the reduction efficiency of Grx (36) and thus the PtTrx*h*4 reduction by these mutants. In contrast, Grx C30S (in which the second cysteine of the active site is removed) was still able to reduce PtTrx*h*4, suggesting that monothiol Grx may be able to interact with this kind of Trx.

The interactions between Trxs and PrxQ were also investigated by measuring H_2O_2 disappearance in the presence of DTT (Fig. 2*b*). Again, the mutant C58S is totally inactive in this system, consistent with the hypothesis that Cys^{58} is the catalytic cysteine. The PtTrx*h*4C61S mutant exhibited a much lower activity than PtTrx*h*4, showing the importance of Cys^{61} in target protein reduction by PtTrx*h*4. In contrast to the results obtained when glutaredoxin was used as the reductant, the PtTrx*h*4C4S mutant is fully active when DTT is the donor.

Overall Description and Structure Comparison of Wild Type PtTrxh4 and PtTrxh4C61S—The two PtTrx*h*4 structural models presented in this study contain intramolecular disulfide bonds involving the catalytic Cys^{58} and either Cys^{61} (WT PtTrx*h*4, despite the crystallization in the presence of DTT) or Cys^{4} (PtTrx*h*4C61S mutant). Here, unless indicated otherwise, structure A refers to the WT PtTrx*h*4 (Fig. 3*a*) and structure B to the PtTrx*h*4C61S mutant (Fig. 3*b*). Generally, both forms of PtTrx*h*4 structures retain the overall thioredoxin fold, which is shared by all members of the thiol-disulfide oxidoreductase family, with a five-stranded β sheet surrounded by four α helices in a $\beta\alpha$ $\beta\alpha$ $\beta\alpha$ $\beta\beta\alpha$ topology (Fig. 3, *a* and *b*).

In structure A, the electron density is well defined along the main chains and for most of the side chains except that the 23 most N-terminal and the 5 most C-terminal amino acids of the WT enzyme could not be located due to weak electron densities, suggesting a high degree of structural flexibility of these parts of the molecule. Hence, this structural model comprises residues 24–134 of PtTrx*h*4. Nevertheless, the full-length of the protein was verified by mass spectroscopy. The oxidized form A is present as two monomers in the asymmetric unit with active site regions facing each other. The active site architecture is similar to that of other known Trxs (37–40). One side of the redox-active disulfide bond is flat and rather hydrophobic (formed by residues Ala^{55}, $^{59}GP^{60}$, $^{99}ATP^{101}$, $^{116}VGA^{118}$; named as hydrophobic site 1; Fig. 3*c*), whereas the other side is more shielded with a pitcher-like predominantly hydrophobic cleft (this cleft is formed by Val^{26}, Leu^{28}, Asn^{52}, Ser^{54}, $^{64}IAP^{66}$cleft, $^{68}YI^{69}$, Val^{82}, Phe^{103}, Leu^{115}, and Leu^{123}; named as hydrophobic site 2; Fig. 3*d*). At the edge of the pitcher-like cleft lies a positively charged patch, $^{56}RW^{57}$ and Lys^{62}. The hydrophobic site 2 accommodates hydrophobic residues from the symmetry-related second monomer.

B structure consists of 129 amino acids (residues 2–139, excluding residues from 7 to 15) and the protein crystallizes as a monomer in the asymmetric unit. Upon formation of the Cys^{4}–Cys^{58} disulfide bond, the active site of form B is covered by the N-terminal extension. The electron density between residues 7 and 15 was barely visible, so no residue was assigned to this assumed highly flexible loop region. Nevertheless, the disulfide bond is undoubtedly present (Fig. 3*b*). The N-terminal is kinked from the rest of the molecule at the double-glycine region ($^{23}GG^{24}$) and this extension is further stabilized by making extensive hydrophobic interactions that involve residues Ile^{19} and $^{21}LAGG^{24}$ with the residues located at hydrophobic site 2. Apart from the hydrophobic interactions, the N-terminal extension is also stabilized by hydrogen bonding (V26N–G23O, I19N–P17O, T100N–C4O, C4N–T100O, A118N–G2O, I19O–R56N-η1). Upon closure of the N-terminal region toward the core of the protein, the molecular surface properties of hydrophobic site 1 remains unchanged (just as described in structure A, see Fig. 3, *c* and *e*, for comparison). However, hydrophobic site 2 pocket is shielded by residues from the N-terminal extension (Pro^{17}–Gly^{24}) and therefore its depth is greatly reduced (see Fig. 3, *d* and *f*, for comparison). Indeed, half of the pitcher-like cleft wall (hydrophobic site 2) has now become more hydrophilic in the B structure (Fig. 3*f*).

If the first 23 amino acids are excluded, superimposition of forms A and B structures yield root mean square deviation values of 0.6 Å (for 110 common Cα atoms). The positions of the active site cysteines (or Ser^{61} in form B structure) remain unchanged in both structures. The A and B structures exhibit different conformations in their active site regions with the most obvious difference observed at residue Trp^{57}. In the B structure, the position of Trp^{57} (χ_1 value = +50.01°, residue stabilized by making a hydrogen bond with the $O_{\delta 2}$ atom of a conserved residue Asp^{86}) is the same as in most of other classical Trxs (χ_1 values between +40° and +55°) and its side chain covers an important part of the active site (Cys^{4}–Cys^{58} disulfide bond) surface. This residue has been shown to be important for the Trx-protein interaction or recognition (41, 42). In contrast, the plane of the indole ring of Trp^{57} (χ_1 value = −81.87°) in the A structure has to "flip out" by about 90° with respect to its usual position as described in the B structure and orients toward the surface of the protein. In the A structure, the Trp^{57} residues of the two independent monomers are facing each other. This residue possesses an elevated average B factor (72.55 $Å^2$) and the indole side chain lacks electron density, suggesting the flexibility of the side chain. Fig. 4 displays a superimposition of the active site region close-up view of form A PtTrx*h*4, form B PtTrx*h*4, and other Trx structures, highlighting the position and orientation of the active site Trp residue. The atypical position of Trp^{57} in structure A is not retained in structure B mainly due to the constraint of the N-terminal.

Apart from the flexibility of Trp^{57}, superimposition of monomers of the A and B structures also revealed that its neighboring residue, Arg^{56}, also possesses a certain degree of mobility. This side chain has moved in toward the molecule by about 40° when comparing the A and B structures. The movements of these two residues actually make way for the N-terminal extension of PtTrx*h*4 to gain access to the active site of the enzyme. Another difference between the two forms is the direction of the side chain of Ser^{54}. Contrary to the A structure where it is more solvent-exposed, the O-γ atom of Ser^{54} is hydrogen bonded to

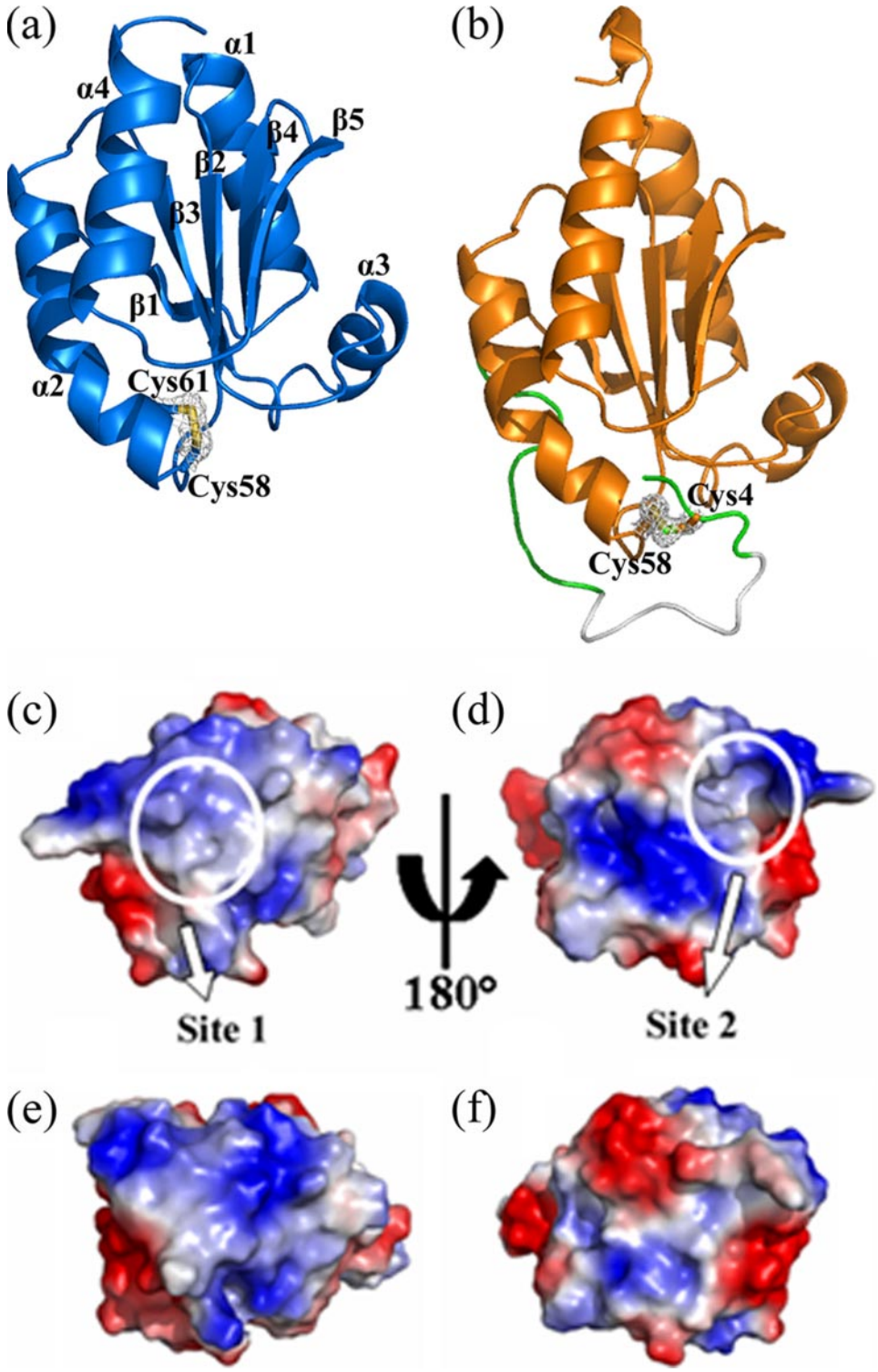

FIGURE 3. **Overall structures of the WT PtTrx*h*4 (*blue*) and the PtTrx*h*4C61S (*orange*) in schematic representation (*a* and *b*) and the electrostatic potential surface charges of the WT (*c* and *d*) and PtTrx*h*4C61S mutant (*e* and *f*), viewing from both sides of the molecule (rotated by 180°).** Molecules in *c–f* correspond to the orthogonal view of the molecule in *a*. For *a* and *b*, the intramolecular disulfide bond in each structure is highlighted, with final $2F_o - F_c$ electron density (1.2 σ level) covering chosen residues for clarity. The N-terminal extension (residues 1–23) is not modeled in the WT PtTrx*h*4 structure (*a*) due to the lacking of electron density, whereas in the PtTrx*h*4C61S partial of the N-terminal extension (residues 2–6 and 16–24, colored in *green*) can be assigned to the structure (*b*, see text for details). In the latter structure, lacking residues (7–15) are shown in an imaginary *gray loop* for a better overview of the structure. Relevant residues and secondary structures are labeled. Two hydrophobic sites, site 1 (*c*) and site 2 (*d*), are *circled* for clarity. Corresponding sites in the mutant can be found in the *bottom panel* (*e* and *f*). Notice that the site 1 cleft is shallower than the pitcher-like hydrophobic site 2 (for WT PtTrx*h*4). The figure was prepared using PyMOL.

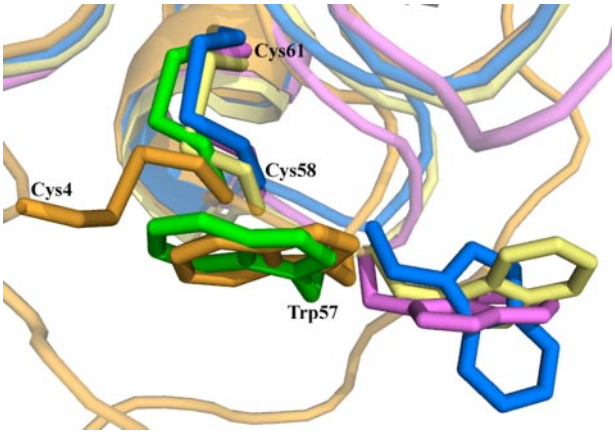

FIGURE 4. **Superimposition of the active site cysteines and tryptophan from poplar WT PtTrx*h*4 (*blue*) (PDB code 3D21) and poplar PtTrx*h*4C61S (*orange*) (PDB code 3D22), *C. reinhardtii* (*green*) (PDB code 1EP7), *T. brucei* (*yellow*) (PDB code 1R26), and spinach Trx*f* short form (*pink*) (PDB code 1F9M).** For PtTrx*h*4, Cys^{58} is the catalytic cysteine (corresponding to Cys-36_{1EP7}, Cys-46_{1F9M}, and Cys-30_{1R26}), Cys^{61} is the first resolving cysteine (corresponding to Cys-39_{1EP7}, Cys-49_{1F9M}, and Cys-33_{1R26}), whereas Cys^{4} is the additional N-terminal cysteine or the second resolving cysteine in the proposed atypical mechanism of PtTrx*h*4 (see text for details). In contrast to the typical position in most Trxs, exemplified by Trp^{35} of green algae Trx *h* (*green*) and Trp^{57} of poplar WT PtTrx*h*4 (*blue*), the Trp^{57} of the PtTrx*h*4C61S mutant has a flipped-out position. The unusual Trp side chain position seen in PtTrx*h*4 has also been found in two other Trx structures mentioned in the text (Trp-45_{1F9M} and Trp-29_{1R26}). The figure was prepared using PyMOL.

the O-δ1 atom of Asn^{52} (~2.7 Å) in the B structure. In this structure, the O-γ atom of Ser^{54} is also hydrogen bonded to the S-γ atom (~3 Å) of Ser^{61} (this residue is originally a cysteine residue). Ser^{54} is highly conserved in PtTrx*h*4 homologues, but usually replaced by a threonine in other plant *h*-type Trxs or an aromatic residue (Phe or Trp) in other non-*h*-type Trxs.

Comparison with Other Trxs—Numerous Trx structures (from different organisms) are known, and all display a high degree of structural homology. Among the plant *h*-type Trxs, there are 4 structures of the plant subgroups 1 and 2 available in the PDB to date (they comprise both NMR and x-ray structures), which show very little differences with other known Trx structures. Therefore, we limit the structure comparison here with *h*-type Trxs unless mentioned otherwise.

Structures alignment with 100–109 Cα showed the root mean square deviation values ranging from 1.0 to 1.6 Å, with Trx *h* of *Chlamydomonas reinhardtii* (green alga, PDB code 1EP7, Ref. 40), Trx *h*2 of *Hordeum vulgare* (barley, PDB code 2IWT, Ref. 43), Trx *h*1 of *A. thaliana* (mouse-ear cress, PDB code 1XFL, Ref. 11) and Trx *h*1 of *P. tremula* (poplar tree, PDB code 1TI3, Ref. 10). Sequence identity among plant *h*-type Trxs mentioned above ranged between 30 and 35% (50–57% of sequence homology). The main differences are located on the extended N-terminal sequence of PtTrx*h*4, which is absent in *h*-type Trxs of subgroups 1 and 2. Nevertheless, the canonical active site motif of Trx, WC*XXC* (*X* can be any amino acid), is present. Interestingly, another motif that involves a conserved cis-proline residue, ^{79}AMP^{81} (numbering in poplar Trx *h*1), is well conserved in all plant Trxs mentioned above and also in most other Trxs from different organisms, but is replaced by an ^{99}ATP^{101} motif in PtTrx*h*4 and its plant orthologs. The positioning of Thr^{100} in PtTrx*h*4 near the disulfide bond (the O-γ1 of Thr^{100} is less than 4 Å away from the S-γ of the catalytic Cys^{58}) and also near hydrophobic site 2, also suggests an important role for this residue.

A noticeable difference between PtTrx*h*4 and other Trx structures is that Val^{82} of PtTrx*h*4, which is situated in the hydrophobic site 2 mentioned earlier (see previous section) is replaced by a lysine residue in all other Trxs (corresponding to Lys^{57} in *E. coli* Trx). In all plant Trxs *h* of subgroup 3, a hydrophobic and relatively small residue is always present. This substitution underlines the hydrophobicity of site 2, whereas in other Trxs a positively charged residue (Lys^{57}) changes the properties of the cavity. In classical Trxs, the corresponding cavity is more solvent-exposed, whereas in PtTrx*h*4, Ser^{54} is the most hydrophilic and polar residue embedded at the bottom of the hydrophobic site 2. All these results suggest that the "hydrophobic cavity" at hydrophobic site 2 may be involved in regulating the flipping of the N-terminal extension of PtTrx*h*4. Indeed, site 2 is complementarily covered by the N-terminal extension in form B structure.

Another peculiarity of the active site of PtTrx*h*4 is the absence of a buried carboxylate behind the active site cysteines. Instead of the common aspartate residue, this corresponding position is occupied by Asn^{52} in PtTrx*h*4 with an equivalent conformation. The buried Asp^{26} carboxyl (using the *E. coli* Trx numbering) and Lys^{57} ϵ-amino groups mentioned, which are in equivalent positions of residues Asn^{52} and Val^{82} in PtTrx*h*4, are suggested to have significantly modulating the pK_a values of the active site thiols, thereby enhancing the rates of thiol-disulfide reactions at physiological pH (45). In other words, the substitution of these two highly conserved residues of Trxs in PtTrx*h*4 and its orthologs may be responsible for the deviation observed in the more electropositive redox potentials. The substitution of the conserved Asp (but above mentioned Lys remains conserved) by another residue in PtTrx*h*4, has also been reported for *Anabaena* Trx-2 (replaced by Tyr^{26}) (46) and for *Trypanosoma* Trx (replaced by Trp^{24}) (47). However, no pK_a values of the active site thiols of these proteins have been determined experimentally.

DISCUSSION

Uniqueness of PtTrxh4—All plant Trxs characterized up to now are reduced by either NTR or ferredoxin/thioredoxin reductase except for poplar thioredoxin PtTrx*h*4 (6). To date, PtTrx*h*4 is the only characterized Trx that is reduced by the GSH/Grx system *in vitro*. It was thus of interest to examine the reasons for the original properties of this Trx. Three conserved cysteines are present in PtTrx*h*4, two found in the classical Trx active site (WCGPC) (Cys^{58} and Cys^{61}, respectively) and one localized in the N-terminal part of the protein (Cys^{4}). Cys^{4}, shown to play a role in the catalytic mechanism in this study, is a well conserved residue found at the same position in all other Trxs of subgroup 3 to which PtTrx*h*4 belongs (8).

Proposed Catalytic Mechanism for an Atypical Thioredoxin—Based on the biochemical and structural data described here, we propose a four-step mechanism for the reaction of reduced PtTrx*h*4 with an oxidized target protein (*e.g.* PrxQ) and its regeneration (Fig. 5). As for other Trxs, catalysis proceeds through the formation of a heterodimer between the target pro-

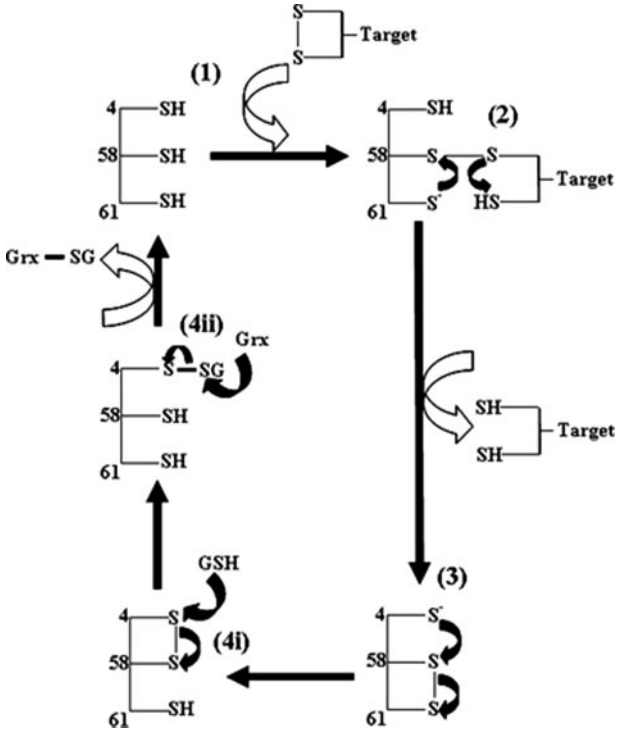

FIGURE 5. **A proposed four-step disulfide cascade mechanism for Grx-dependent PtTrx*h*4 catalysis.** *1*) Cys^{58} attacks initially the S-γ atom of an oxidized target protein; *2*) the heterodisulfide is then reduced by the active site recycling cysteine (Cys^{61}); *3*) the resulting disulfide bond (Cys^{58}–Cys^{61}) is further reduced by the second recycling cysteine, Cys^4; and *4i*) a glutathione molecule (GSH) reduces the Cys^4–Cys^{58} disulfide bond prior to, *4ii*, the final nucleophilic attack of the Trx-SG adduct by the catalytic Cys of monothiol or dithiol Grx.

tein and PtTrx*h*4 involving the catalytic Cys^{58}. The hetero-disulfide is then cleaved by Cys^{61}, leading to the release of the reduced target protein and the formation of a disulfide bond between Cys^{58} and Cys^{61} visible in the WT PtTrx*h*4 crystal structure (this step is identical to the one that has been documented for other Trxs). Then, the N-terminal Cys^4 is involved in a nucleophilic attack on the Cys^{58}–Cys^{61} disulfide bond, leading to the formation of a second intramolecular disulfide bond between Cys^4 and Cys^{58}. The oxidized protein can then be reduced by the Grx/GSH system. In this atypical Trx mechanism, the thiolate of Grx is proposed to initiate a nucleophilic attack on the Cys^4-glutathionylated Trx, leading to the release of fully reduced Trx. The latter steps of this reaction have not been reported in other Trxs and are discussed further below.

Cys^4 of PtTrxh4 Acts as the Second Resolving Cysteine—From the activity assay results (Fig. 2*a*), we know that PtTrx*h*4C4S is nearly as inactive as the PtTrx*h*4C58S when the Grx/GSH system is used as a reductant. In structure B, we observed that (i) PtTrx*h*4 can form a disulfide bond between Cys^4 and Cys^{58}, (ii) this disulfide bond is non-artifactual because the N-terminal extension fits perfectly in the hydrophobic site 2 pocket by complementary matching involving invariant residues of subgroup 3 Trxs *h*, (iii) Cys^{61} is unlikely to attack the disulfide bond because it is totally buried in the enzyme, and (iv) Cys^4 is the only solvent-accessible cysteine, suggesting that it is able to interact with the electron donor. This study suggests that Cys^4 acts as the second recycling cysteine by reducing the Cys^{58}–Cys^{61} disulfide bond, leading to the formation of a second intramolecular disulfide bond, *i.e.* Cys^4–Cys^{58}. The catalytic mechanism proposed for PtTrx*h*4 is related to the one described for some peptide methionine sulfoxide reductases A (MsrA), whereupon catalysis of three cysteines form two consecutive intramolecular disulfide bonds before the regeneration of the enzyme by Trxs (48).

PtTrxh4 Is Regenerated by a GSH/Grx Reducing System but Not by the Typical NTR Reducing System—In terms of redox potential, WT PtTrx*h*4 (E_m average value of −165 mV, see "Results") should be reducible by the NTR reducing system as demonstrated for the vast majority of the Trxs (E_m values in the −280 to −310 mV range observed for other Trxs (6, 7, 49)). Thus, there must be reasons other than thermodynamic driving force for the inability of NTR to regenerate PtTrx*h*4. The superimposition with the structure of the Trx-NTR complex (PDB code 1F6M) (50), reveals that the N-terminal extension of PtTrx*h*4 is preventing the interaction with NTR. In addition, structure B exhibits a highly negatively charged molecular surface around the active site that may disfavor its interaction with NTR, which also possesses a negatively charged active site surface. Clearly, the N-terminal part of PtTrx*h*4 is not the only determinant responsible for the lack of reactivity with NTR because the [SeMet]PtTrx*h*4 (truncated form, consisting of residues Asn^{25} to Met^{134}) is also not reduced either by *A. thaliana* or *E. coli* NTR.

The conformation of the side chain of Trp^{57} at the active site (WC*XX*C) may also play an important role in preventing a productive interaction between PtTrx*h*4 and NTR. Although the major role of this residue is related to substrate/Trx recognition and interaction (41, 42, 51), it is also involved in the Trx/TrxR interaction (50). In both A (WT and [SeMet]PtTrx*h*4) and B (PtTrx*h*4C61S) structures, the side chain of Trp^{57} shows a high flexibility, so that it can either be close to the disulfide bond (structure B) or somewhat distant from the disulfide bond (structure A). A similar flexibility of the corresponding tryptophan has been reported for other Trxs that do not use the common NTR reducing system: the spinach chloroplastic Trx *f* (short form), which uses the ferredoxin/thioredoxin reductase system for its reduction (52) and the Trx of *Trypanosoma brucei* (Fig. 4), which is spontaneously reduced by the trypanothione/trypanothione reductase system of this parasite (53). These interesting reports hint that Trxs with increased flexibility for this conserved Trp most likely use regeneration system(s) other than the NTR reducing system.

One point that is still unclear is whether the Cys^4–Cys^{58} disulfide bond, once formed, is reduced by GSH or by Grx. In terms of redox potential, an E_m value of −165 mV for PtTrx*h*4 is fully compatible with its thermodynamically favorable complete reduction by either glutathione (GSH/GSSG, E_m value of −241 mV) (54) or glutaredoxins (E_m values of −233, −198 mV and −170 ± 10 mV for *E. coli* Grx1, *E. coli* Grx3, and plant Grx C4, respectively) (55–57). We show here that neither GSH nor Grx alone can complete the regeneration of the enzyme but both together are essential for the catalytic mechanism. The fact that we have not been able to obtain a complex between a mutated PtGrx C30S and the PtTrx*h*4C61S suggests that the possibility of direct reduction by Grx is unlikely. It is interesting

to note that PtTrx*h*4 can be easily glutathionylated *in vitro* (using mass spectrometry to characterize tryptic digests of glutathionylated WT PtTrx*h*4). Hence, we can postulate that the reaction with a GSH molecule occurs prior to the reaction with Grx in the catalytic cycle.

Physiological Considerations of PtTrxh4—Orthologs of PtTrx*h*4 are also present in different plants. Based on amino acid sequence comparisons, it seems quite reasonable to assume that these proteins should, like PtTrx*h*4, be able to use Grx as an electron donor. This assumption is consistent with the report that the *Phalaris coerulescens* ortholog is not reduced by NTR (9). It has been shown that ribonucleotide reductase cannot use monothiol Grx as donor, whereas other reactions catalyzed by Grx require either monothiol or dithiol Grxs (55, 58, 59). Based on these considerations, it is tempting to speculate that both kinds of Grx may be able to promote the activity of PtTrx*h*4 and its orthologs. Moreover, there are many naturally occurring monothiol Grx in plants. It will be of considerable interest to compare the relative efficiencies of the corresponding proteins for PtTrx*h*4 catalysis.

The physiological role of this particular kind of GSH/Grx reducible Trx remains to be elucidated. Although PtTrx*h*4 is unable to reduce several isoforms of poplar glutathione peroxidases,[4] the enzyme is capable of reducing a cytosolic MsrA and a Prx II from poplar (8). In a recent study, it has been shown that *A. thaliana* NTR knock-out mutants are viable and fertile and that the inactivation of NTR could be compensated by pathways linked to GSH (44). It is tempting to speculate that this particular subgroup of Trx reduced by Grxs could be involved in this compensatory mechanism. Preliminary experiments suggest that PtTrx*h*4 is expressed both at transcriptional and protein levels in different poplar tissues.[5] Further studies are required to identify other possible targets, keeping in mind that the E_m value of PtTrx*h*4 is significantly more positive than that of most Trxs and thus thermodynamic considerations would limit the number of protein disulfides that PtTrx*h*4 is capable of reducing.

Acknowledgments—We thank F. Favier for careful reading of the manuscript. We are very grateful to the FIP team in ESRF, Grenoble, France, and the DESY team in EMBL-Hamburg Outstation, Germany, for providing access to beamlines BM30A, X11, and BW7A.

REFERENCES

1. Meyer, Y., Vignols, F., and Reichheld, J. P. (2002) *Methods Enzymol.* **347,** 394–402
2. Schürmann, P. (2003) *Antiox. Redox Signal.* **5,** 69–78
3. Gelhaye, E., Rouhier, N., Navrot, N., and Jacquot, J. P. (2004) *Cell Mol. Life Sci.* **62,** 24–35
4. Laloi, C., Rayapuram, N., Chartier, Y., Grienenberger, J. M., Bonnard, G., and Meyer, Y. (2001) *Proc. Natl. Acad. Sci. U. S. A.* **98,** 14144–14149
5. Gelhaye, E., Rouhier, N., Navrot, N., and Jacquot, J. P. (2004) *Plant Physiol. Biochem.* **42,** 265–271
6. Bréhélin, C., Laloi, C., Setterdahl, A. T., Knaff, D. B., and Meyer, Y. (2004) *Photosynth. Res.* **79,** 295–304
7. Gelhaye, E., Rouhier, N., Gerard, J., Jolivet, Y., Gualberto, J., Navrot, N., Ohlsson, P. I., Wingsle, G., Hirasawa, M., Knaff, D. B., Wang, H., Dizengremel, P., Meyer, Y., and Jacquot, J. P. (2004) *Proc. Natl. Acad. Sci. U. S. A.* **101,** 14545–14550
8. Gelhaye, E., Rouhier, N., and Jacquot, J. P. (2003) *FEBS Lett.* **555,** 443–448
9. Juttner, J., Olde, D., Langridge, P., and Baumann, U. (2000) *Eur. J. Biochem.* **267,** 7109–7117
10. Coudevylle, N., Thureau, A., Hemmerlin, C., Gelhaye, E., Jacquot, J. P., and Cung, M. T. (2005) *Biochemistry* **44,** 2001–2008
11. Peterson, F. C., Lytle, B. L., Sampath, S., Vinarov, D., Tyler, E., Shahan, M., Markley, J. L., and Volkman, B. F. (2005) *Protein Sci.* **14,** 2195–2200
12. Jacquot, J. P., Rivera-Madrid, R., Marinho, P., Kollarova, M., Le Marechal, P., Miginiac-Maslow, M., and Meyer, Y. (1994) *J. Mol. Biol.* **235,** 1357–1363
13. Rouhier, N., Gelhaye, E., Gualberto, J. M., Jordy, M. N., De Fay, E., Hirasawa, M., Duplessis, S., Lemaire, S. D., Frey, P., Martin, F., Manieri, W., Knaff, D. B., and Jacquot, J. P. (2004) *Plant Physiol.* **134,** 1027–1038
14. Rouhier, N., Gelhaye, E., and Jacquot, J. P. (2002) *J. Biol. Chem.* **277,** 13609–13614
15. Rouhier, N., Gelhaye, E., Sautiere, P. E., and Jacquot, J. P. (2002) *Protein Expression Purif.* **24,** 234–241
16. Schenk, P. M., Baumann, S., Mattes, R., and Steinbiss, H. H. (1995) *BioTechniques.* **19,** 196–200
17. Navrot, N., Collin, V., Gualberto, J., Gelhaye, E., Hirasawa, M., Rey, P., Knaff, D. B., Issakidis, E., Jacquot, J. P., and Rouhier, N. (2006) *Plant Physiol.* **142,** 1364–1379
18. Krimm, I., Lemaire, S., Ruelland, E., Miginiac-Maslow, M., Jacquot, J. P., Hirasawa, M., Knaff, D. B., and Lancelin, J. M. (1998) *Eur. J. Biochem.* **255,** 185–195
19. Hirasawa, M., Ruelland, E., Schepens, I., Issakidis-Bourguet, E., Miginiac-Maslow, M., and Knaff, D. B. (2000) *Biochemistry* **39,** 3344–3350
20. Masuda, S., Dong, C., Swem, D., Knaff, D. B., and Bauer, C. E. (2002) *Proc. Natl. Acad. Sci. U. S. A.* **99,** 7078–7083
21. Deiana, L., Carru, C., Pes, G., and Tadolini, B. (1999) *Free Radic. Res.* **31,** 237–244
22. Otwinowski, Z., and Minor, W. (1997) *Methods Enzymol.* **276,** 307–326
23. Kabsch, W. (1993) *J. Appl. Crystallogr.* **26,** 795–800
24. CCP4 Collaborative Computational Project Number 4 (1994) *Acta Crystallogr. Sect. D Biol. Crystallogr.* **50,** 760–763
25. Sheldrick, G. M., and Schneider, T. R. (1997) *Methods Enzymol.* **277,** 319–343
26. de La Fortelle, E., and Bricogne, G. (1997) *Methods Enzymol.* **276,** 472–494
27. Abrahams, J. P., and Leslie, A. G. (1996) *Acta Crystallogr. Sect. D Biol. Crystallogr.* **52,** 30–42
28. Perrakis, A., Morris, R., and Lamzin, V. S. (1999) *Nat. Struct. Biol.* **6,** 458–463
29. Roussel, A., and Cambillau, C. (1989) *Silicon Graphics Geometry Partners Directory*, pp. 77–78, Silicon Graphics, Mountain View, CA
30. Vagin, A., and Teplyakov, A. (1997) *J. Appl. Crystallogr.* **30,** 1022–1025
31. Brünger, A. T., Adams, P. D., Clore, G. M., DeLano, W. L., Gros, P., Grosse-Kunstleve, R. W., Jiang, J. S., Kuszewski, J., Nilges, M., Pannu, N. S., Read, R. J., Rice, L. M., Simonson, T., and Warren, G. L. (1998) *Acta Crystallogr. Sect. D Biol. Crystallogr.* **54,** 905–921
32. Emsley, P., and Cowtan, K. (2004) *Acta Crystallogr. Sect. D Biol. Crystallogr.* **60,** 2126–2132
33. Laskowski, R. A., MacArthur, M. W., Moss, D. S., and Thornton, J. M. (1993) *J. Appl. Crystallogr.* **26,** 283–291
34. DeLano, W. L. (2002) *The PyMOL Molecular Graphics System,* DeLano Scientific, Palo Alto, CA
35. Kleywegt, G. J., and Jones, T. A. (1997) *Acta Crystallogr. Sect. D Biol. Crystallogr.* **53,** 179–185
36. Rouhier, N., Gelhaye, E., and Jacquot, J. P. (2002) *FEBS Lett.* **511,** 145–149
37. Holmgren, A., Söderberg, B. O., Eklund, H., and Brändén, C. I. (1975) *Proc. Natl. Acad. Sci. U. S. A.* **72,** 2305–2309
38. Katti, S. K., LeMaster, D. M., and Eklund, H. (1990) *J. Mol. Biol.* **212,** 167–184
39. Weichsel, A., Gasdaska, J. R., Powis, G., and Monfort, W. R. (1996) *Structure* **4,** 735–751

[4] N. Navrot, unpublished results.
[5] N. Rouhier, unpublished results.

40. Menchise, V., Corbier, C., Didierjean, C., Saviano, M., Benedetti, E., Jacquot, J. P., and Aubry, A. (2001) *Biochem. J.* **359,** 65–75
41. Menchise, V., Corbier, C., Didierjean, C., Jacquot, J. P., Benedetti, E., Saviano, M., and Aubry, A. (2000–2001) *Biopolymers.* **56,** 1–7
42. Krause, G., and Holmgren, A. (1991) *J. Biol. Chem.* **266,** 4056–4066
43. Maeda, K., Hägglund, P., Finnie, C., Svensson, B., and Henriksen, A. (2006) *Structure* **14,** 1701–1710
44. Reichheld, J. P., Khafif, M., Riondet, C., Droux, M., Bonnard, G., and Meyer, Y. (2007) *Plant Cell* **19,** 1851–1865
45. Dyson, H. J., Jeng, M.-F., Tennant, L. L., Slaby, I., Lindell, M., Cui, D.-S., Kuprin, S., and Holmgren, A. (1997) *Biochemistry* **36,** 2622–2636
46. Saarinen, M., Gleason, F. K., and Eklund, H. (1995) *Structure* **3,** 1097–1108
47. Friemann, R., Schmidt, H., Ramaswamy, S., Forstner, M., Krauth-Siegel, R. L., and Eklund, H. (2003) *FEBS Lett.* **554,** 301–305
48. Boschi-Muller, S., Azza, S., Sanglier-Cianferani, S., Talfournier, F., Van Dorsselear, A., and Branlant, G. (2000) *J. Biol. Chem.* **275,** 35908–35913
49. Wangensteen, O. S., Chueca, A., Hirasawa, M., Sahrawy, M., Knaff, D. B., and Lopez Gorge, J. (2001) *Biochim. Biophys. Acta* **1547,**156–166
50. Lennon, B. W., Williams, C. H., Jr., and Ludwig, M. L. (2000) *Science* **289,** 1190–1194
51. Koh, C. S., Didierjean, C., Navrot, N., Panjikar, S., Mulliert, G., Rouhier, N., Jacquot, J. P., Aubry, A., Shawkataly, O., and Corbier, C. (2007) *J. Mol. Biol.* **370,** 512–529
52. Crawford, N. A., Droux, M., Kosower, N. S., and Buchanan, B. B. (1989) *Arch. Biochem. Biophys.* **271,** 223–239
53. Schmidt, H., and Krauth-Siegel, R. L. (2003) *J. Biol. Chem.* **278,** 46329–46336
54. Cheng, Z., Arscott, L. D., Ballou, D. P., and Williams, C. H., Jr. (2007) *Biochemistry* **46,** 7875–7885
55. Rouhier, N., Gelhaye, E., and Jacquot, J. P. (2004) *Cell Mol. Life Sci.* **61,** 1266–1277
56. Aslund, F., Berndt, K. D., and Holmgren, A. (1997) *J. Biol. Chem.* **272,** 30780–30786
57. Rouhier, N., Unno, H., Bandyopadhyay, S., Masip, L., Kim, S. K., Hirasawa, M., Gualberto, J. M., Lattard, V., Kusunoki, M., Knaff, D. B., Georgiou, G., Hase, T., Johnson, M. K., and Jacquot, J. P. (2007) *Proc. Natl. Acad. Sci. U. S. A.* **104,** 7379–7384
58. Fernandes, A. P., and Holmgren, A. (2004) *Antioxid. Redox Signal.* **6,** 63–74
59. Bushweller, J. H., Åslund, F., Wüthrich, K., and Holmgren, A. (1992) *Biochemistry* **31,** 9288–9293